Evolution of Crystallinity, Chain Mobility, and Crystallite Size during Polymer Crystallization

Johannes Leisen* and Haskell W. Beckham

School of Polymer, Textile and Fiber Engineering, Georgia Institute of Technology, Atlanta, Georgia 30332-0295

Mohammed A. Sharaf

Department of Chemistry, Helwan University, Ain Helwan, Egypt

Received May 20, 2004; Revised Manuscript Received August 9, 2004

ABSTRACT: A ^{1}H NMR method is described for examining crystallinity, chain mobility, and crystallite size in real time during polymer crystallization. The method is demonstrated by following the crystallization of natural rubber at −10 °C. At selected stages during the crystallization, a Bloch decay was recorded along with Goldman−Shen decays for a series of mixing times using a filter duration to destroy the rigid-phase magnetization. The fast-relaxing components of the Bloch and Goldman−Shen decays correspond to the rigid/crystalline fraction of the sample and were fitted to Gaussian functions. The slow-relaxing components were obtained experimentally using the Goldman−Shen sequence measured with a short mixing time (1 ms). By combining the fitted Gaussian portions with the experimentally determined slow-relaxing components, the Bloch and Goldman−Shen decays could be analyzed across the entire crystallization process. The Bloch decays provided information on the amount and nature of the rigid fraction, while the Goldman−Shen spin-diffusion data provided information on domain size. The formation of noncrystalline rigid domains was observed for the initial stages of the crystallization process. Data clearly indicate lateral growth of crystallites with relatively uniform thickness during the primary crystallization process. Later stages of crystallization are characterized by increasing heterogeneity in crystalline density and perfection.

Introduction

Crystallites in polymers exhibit a major influence on their bulk properties.[1] Modifications to crystallinity can significantly alter mechanical or optical properties, for example. Thus, the thermal history of a polymer, in particular the details of its experience between T_g and T_m,[2,3] greatly influences its end-use value. Hence, polymer crystallinity is characterized on a routine basis. Particularly useful analytical techniques allow the determination of both crystallite size and overall crystallinity in real time for kinetic studies. For mechanical properties above T_g, characterization of the interface between the mobile amorphous domains and a rigid phase such as a filler or a crystallite is also of interest.[4]

When the densities of amorphous and crystalline phases are known, crystallization processes in polymers may be followed by simple dilatometric techniques.[5] Crystals growing in thin films may be readily observed with optical microscopy[6] and light scattering techniques.[7,8] These techniques can be used to determine the total amount and morphology of crystals, including formation kinetics. Molecular-level information on crystallite structure can be obtained by X-ray[9,10] or electron diffraction methods.[11] However, if kinetics are measured with X-ray techniques, it is often necessary to use expensive synchrotron radiation sources.[12]

Methods of nuclear magnetic resonance (NMR) have been used successfully to characterize the crystalline structure within many polymeric materials.[13−23] In fact, relatively cost-effective low-resolution NMR scanners are used routinely to determine crystallinity in semicrystalline commodity polymers.[24] The nucleus of choice is typically the ^{1}H, whose sensitivity along with modern pulsed NMR instrumentation allows the measurement of % crystallinity in seconds or less. Hence, simple ^{1}H NMR experiments may be used for time-resolved studies of polymer crystallization.[13,14,20,22] These studies are based on measuring Bloch decays, which are then fitted to relaxation functions containing adjustable parameters that describe the relative amounts and nature of the underlying domains in the sample. When the crystalline, amorphous, and interphase domains are considered, up to eight fit parameters are required.[19] This approach provides a wealth of information but is also associated with considerable ambiguity due to the use of so many adjustable parameters.

Here we present a novel, very robust, and yet simple approach for investigating polymer crystallization by ^{1}H NMR using fit functions composed of only three adjustable parameters.[25] In addition to Bloch decays, spin-diffusion data[26] are also measured at a given stage of polymer crystallization. Thus, in addition to the total crystalline content, the crystallite size may be determined as a function of crystallization time. Even though it is not considered explicitly, our approach also provides insight into the nature of the interface between amorphous and crystalline domains. The method is demonstrated for crystallization of natural rubber at −10 °C. However, the experimental approach described here is anticipated to be of general use for the characterization of crystallization processes in protonated polymers.

NMR Experiments

For a semicrystalline polymer sample above its glass transition, the fraction of amorphous and crystalline

* Corresponding author: e-mail johannes.leisen@ptfe.gatech.edu.

10.1021/ma0489974 CCC: $27.50
Published on Web 09/18/2004

phases may be simply obtained by deconvolution of a time-dependent Bloch decay, $I_{\mathrm{Bloch}}(t)$:

$$I_{\mathrm{Bloch}}(t) = w_{\mathrm{mobile}}F_{\mathrm{mobile}}(t) + w_{\mathrm{rigid}}F_{\mathrm{rigid}}(t) \qquad (1)$$

The fast-decaying component, $F_{\mathrm{rigid}}(t)$, is attributed to rigid crystallites while the slow-relaxing component, $F_{\mathrm{mobile}}(t)$, is due to the mobile amorphous phase. Data can be normalized such that w_{rigid} and w_{mobile} represent molar fractions of mobile and rigid phases, respectively (i.e., $w_{\mathrm{mobile}} + w_{\mathrm{rigid}} = 1$). Equation 1 neglects contributions from an interphase; evaluation of crystallinity in polymers based on this simplified two-phase model has been proven feasible.[13,27,28] For kinetic studies, a suitable model function for $I_{\mathrm{Bloch}}(t)$ should describe the changes in the free-induction decays observed experimentally over the entire crystallization process and for a wide range of experimental conditions (e.g., different temperatures).

On the time scale of the NMR experiment, chains within crystallites do not typically exhibit significant amounts of large-angle molecular motions so that ^{1}H−^{1}H dipolar couplings govern the relaxation. Consequently, $F_{\mathrm{rigid}}(t)$ can be modeled by a Gaussian function in which $T^*_{2,\mathrm{rigid}}$ is the decay constant:

$$F_{\mathrm{rigid}}(t) = \exp\left\{-\left(\frac{t}{T^*_{2,\mathrm{rigid}}}\right)^2\right\} \qquad (2)$$

The relaxation of protons in a well-defined crystalline lattice often appears as an FID with some sinusoidal character, the so-called Abragam function.[29] This is certainly the case for semicrystalline polyethylene.[17,30] For the natural rubber investigated here, there were no clear signs of this sinusoidal character in the FID (vide infra, cf. Figure 3). This signifies the absence of well-defined distances between individual protons in the rigid phase. Hence, the existence of small crystallites with large amounts of defects and even rigidified amorphous components is likely for natural rubber.

The natural rubber studied here exhibits a calorimetric T_g at −66 °C (cooling rate of 10 °C/min); crystallization is easily observed from −40 to 10 °C. Over this temperature range, large changes occur for the amorphous phase, making it difficult to adequately model its behavior with a single $F_{\mathrm{mobile}}(t)$. At the lower temperatures from −40 to −20 °C, the molecular motion within the amorphous phase is sufficiently slow that ^{1}H−^{1}H dipolar couplings govern the relaxation. Consequently, $F_{\mathrm{mobile}}(t)$ can be modeled by a Gaussian function similar to that shown in eq 2, but with $T^*_{2,\mathrm{mobile}}$ as the decay constant. At the higher temperatures above −10 °C, large-angle molecular motions occur more rapidly and more frequently, leading to a reduction of any residual dipolar couplings. Consequently, chemically distinguishable nuclei contribute separately to the relaxation function (i.e., chemical shift resolution). A suitable model function may be found for $F_{\mathrm{mobile}}(t)$ under these circumstances, but it will be quite complex. It would also not be general. Because of the chemical shift influences, a model function would depend on the sample, the strength of the external magnetic field, and the excitation frequency. Hence, evaluation of $I_{\mathrm{Bloch}}(t)$ data measured at different temperatures would require the selection of temperature- and spectrometer-dependent fitting functions.

A more general approach is the combination of a theoretical function for $F_{\mathrm{rigid}}(t)$ with experimental data measured for $F_{\mathrm{mobile}}(t)$:

$$I_{\mathrm{Bloch}}(t) = w_{\mathrm{rigid}} \exp\left\{-\left(\frac{t}{T^*_{2,\mathrm{rigid}}}\right)^2\right\} + w_{\mathrm{mobile}}I_{\mathrm{GS}}(t,t_{\mathrm{m}}\rightarrow 0) \qquad (3)$$

The experimental data, $I_{\mathrm{GS}}(t,t_{\mathrm{m}}\rightarrow 0)$, are obtained by selective measurement of slow-relaxing magnetization using a Goldman−Shen (GS) pulse sequence with a filter to destroy the rigid-phase magnetization and a mixing time (t_{m}) that is short enough to prevent significant transfer of magnetization back into the rigid phase.[31] This GS decay corresponds to mobile-phase magnetization and can be attributed to the amorphous fraction within a semicrystalline polymer. At lower temperatures, where a Gaussian decay function like that shown in eq 2 may be applicable for both amorphous- and crystalline-phase magnetization, the $T^*_{2,\mathrm{rigid}}$ of eq 3 must be significantly smaller than the $T^*_{2,\mathrm{mobile}}$ to distinguish between phases. In fact, this condition is essential for any model function chosen for $I_{\mathrm{Bloch}}(t)$ and also for using the GS sequence to selectively measure $F_{\mathrm{mobile}}(t)$.

The Goldman−Shen and other T_2-based filter sequences such as the dipolar filter have been used for the characterization of polymer morphologies.[26] Following application of the filter, the selected mobile-phase magnetization is exposed to a variable-duration mixing time (t_{m}). For very short mixing times, the detected magnetization corresponds to the mobile phase. For longer mixing times, the selected mobile-phase magnetization will transfer to rigid domains via dipolar-coupling-mediated spin diffusion. The amount of mobile-phase magnetization, $m_{\mathrm{mobile}}(t_{\mathrm{m}})$, transferred to the rigid domains for a given mixing time, $m_{\mathrm{rigid}}(t_{\mathrm{m}})$, may be approximated by analyzing the respective GS decay using an equation analogous to eq 3:

$$I_{\mathrm{GS}}(t,t_{\mathrm{m}}) = m_{\mathrm{rigid}}(t_{\mathrm{m}}) \exp\left\{-\left(\frac{t}{T^*_{2,\mathrm{rigid}}}\right)^2\right\} + m_{\mathrm{mobile}}(t_{\mathrm{m}})\, I_{\mathrm{GS}}(t,t_{\mathrm{m}}\rightarrow 0) \qquad (4)$$

For short mixing times (i.e., $t_{\mathrm{m}} \rightarrow 0$), $m_{\mathrm{rigid}}(t_{\mathrm{m}}) = 0$ and $m_{\mathrm{mobile}}(t_{\mathrm{m}}) = 1$. As the mixing time is increased, $m_{\mathrm{rigid}}(t_{\mathrm{m}})$ increases and $m_{\mathrm{mobile}}(t_{\mathrm{m}})$ decreases until complete equilibration of magnetization occurs. At sufficiently long mixing times (i.e., as $t_{\mathrm{m}} \rightarrow \infty$), $I_{\mathrm{GS}}(t,t_{\mathrm{m}})$ assumes the shape of $I_{\mathrm{Bloch}}(t)$ but with lower overall intensity, $m_{\mathrm{mobile}}(t_{\mathrm{m}}) = w_{\mathrm{mobile}}$ and $m_{\mathrm{rigid}}(t_{\mathrm{m}}) = w_{\mathrm{rigid}}$. The spin diffusion data are analyzed by fitting eq 4 to determine $m_{\mathrm{mobile}}(t_{\mathrm{m}})$, which is then plotted as a function of $\sqrt{t_{\mathrm{m}}}$. Following the approach of Mellinger et al.,[32] the initial slope of this plot is extrapolated to $m_{\mathrm{mobile}}(t_{\mathrm{m}}) = 0$ to find t^*_{m}, which is used to calculate the size of the mobile domains. This calculation requires spin-diffusion constants, which can be obtained from the T_2 relaxation time using an established calibration curve.[32]

The determination of polymer crystallinity using eq 3 requires two separate NMR experiments to measure: (1) a Bloch decay and (2) a Goldman−Shen decay. Depending on the T_1 relaxation times and number of data accumulations, these two experiments can be performed within several tens of seconds. If domain sizes are to be determined for a single stage during an ongoing crystallization process, Goldman−Shen data

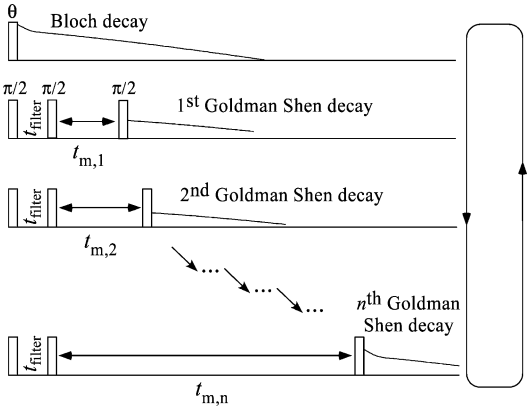

Figure 1. Sequence of experiments used to measure crystallinity, chain mobility, and crystallite size during a single stage of an ongoing polymer crystallization process. A Bloch decay is followed by Goldman−Shen decays with different mixing times. The filter duration on the Goldman−Shen sequence is set to destroy the rigid-phase magnetization; the n^{th} Goldman−Shen decay will be similar in shape to the Bloch decay, but with lower overall intensity. The measurement time for this entire data matrix must be very small compared to the total crystallization time.

need to be recorded for multiple mixing times. This can be typically achieved in several minutes. This time frame is sufficiently short to neglect changes in the nature and amount of growing crystallites for crystallization processes that occur over several hours. The entire experimental sequence is shown in Figure 1.

Analysis of spin-diffusion data based on eq 4 depends on $T^*_{2,\mathrm{rigid}}$, which is the third adjustable fit parameter (in addition to the mobile- and rigid-phase magnetization). This parameter reveals additional and perhaps unanticipated information on semicrystalline polymer morphology. In a sample without an interphase between its crystalline and amorphous domains, crystalline-phase magnetization will be characterized by a single value of $T^*_{2,\mathrm{rigid}}$ that should not change as a function of t_m. A more realistic scenario is that of a sizable interphase. For a polymer between T_g and T_m, chains within the interphase will exhibit mobilities intermediate to mobilities of chains in crystalline and amorphous regions. Consequently, the T_2^* values for an interphase should be greater than those measured for the crystallites. In a spin-diffusion experiment, mobile-phase magnetization must travel through this interphase on its way to the rigid crystalline phase. Since the model function used to fit the GS decays (eq 4) only contains a single T_2^* parameter, $T^*_{2,\mathrm{rigid}}$, the magnitude of this parameter should reflect the relative fraction of interphase in the sample (cf. Figure 2). If a significant interphase exists, it will be most obvious for short mixing times and characterized by a $T^*_{2,\mathrm{rigid}}$ that is greater than the $T^*_{2,\mathrm{rigid}}$ measured for a well-crystallized sample. For longer mixing times, as most of the magnetization has passed through this interphase, the $T^*_{2,\mathrm{rigid}}$ should be more representative of the rigid/crystalline phase. If the relative fraction of interphase to crystalline phase changes as a function of crystallization time, this should be observed as changes in plots of $T^*_{2,\mathrm{rigid}}$ vs mixing time.

Experimental Section

The ^{1}H NMR experiments were conducted on a Bruker DSX 300 spectrometer (Bruker Biospin, Rheinstetten, Germany) at

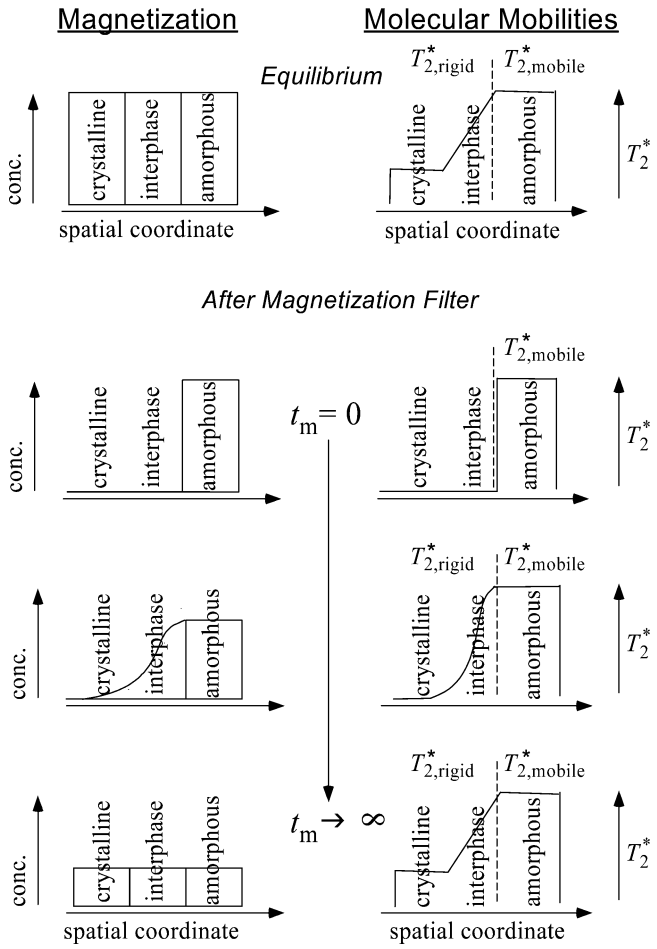

Figure 2. Magnetization pathway in a polymer with an interphase during a spin-diffusion experiment (left column, depicted as relative concentrations) along with the corresponding molecular mobilities (right column, represented by T_2^* values). Note the existence of a distribution of $T^*_{2,\mathrm{rigid}}$ values after spin diffusion carries magnetization into the interphase. Fitting data with eq 4 returns a single value for $T^*_{2,\mathrm{rigid}}$, in which information is embodied on the relative fractions of interphase and crystalline phases.

a magnetic field strength of 7.1 T. A static double-resonance probe with a 7-mm coil was used. The temperature within the probe was controlled using the variable-temperature accessory of the spectrometer. Prior to the NMR measurements, the natural rubber sample was held at 70 °C for about 30 min and then quenched to ensure that no crystallites were present at the beginning of the experiment. Crystallization of the pure natural rubber at −10 °C was observed by ^{1}H NMR spectroscopy for 24 h. Bloch decays were measured and followed immediately by Goldman−Shen experiments (cf. Figure 1) for 16 different mixing times from 1 to 1500 ms. The time required to measure these 17 different decays, referred to here as a "stage" of the crystallization, was about 18 min. Crystallization occurred most rapidly within the first 10 h of the experiment (see Figure 4); during this time, the crystallinity reached nearly 30%, and 30 stages were measured. Thus, during a single stage, the change in the total crystallinity of the sample was less than 1%. Even so, single-stage data sets were not recorded with consecutively increasing values of t_m but with randomly ordered mixing times to avoid errors in data interpretation caused by systematic changes in the sample.

For both the Goldman−Shen and Bloch decays, a repetition delay of 4 s was used, and 512 complex data points were acquired using a dwell time of 1 μs. The Goldman−Shen sequence consisted of three $\pi/2$ pulses with a length of 3 μs. The time interval between the first two pulses, which acts as

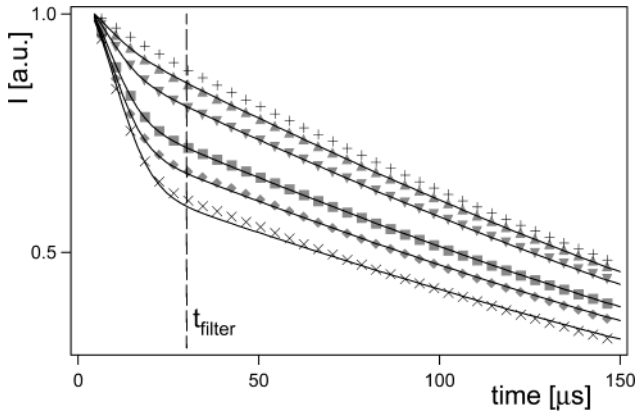

Figure 3. Experimental ^{1}H NMR free-induction decays for semicrystalline natural rubber after crystallization for 24 h at −10 °C: Bloch decay (×) and Goldman−Shen decays recorded using a 30-μs filter duration (marked by vertical dashed line) to destroy rigid-phase magnetization followed by these mixing times, t_m: 1 ms (+), 5 ms (▲), 8 ms (▼), 24 ms (■), and 50 ms (◆). Solid lines are fits to eq 3 (Bloch decay: ×) or eq 4 (Goldman−Shen decays: ▲, ▼, ■, ◆) using the data set $I_{GS}(t,t_m = 1\text{ ms})$ (+) as an approximation for $I_{GS}(t,t_m \rightarrow 0)$. For each data point, errors are less than the symbol sizes.

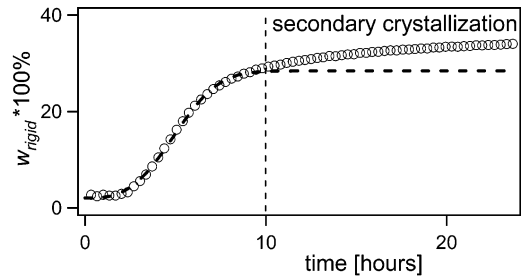

Figure 4. Fraction of rigid components (i.e., crystallites) vs time for the crystallization of natural rubber at −10 °C. The sigmoidal curve is a fit to the initial data using the Avrami equation.[33,34] The slower but continuing increase in crystallinity after about 10 h is indicative of secondary crystallization processes. Experimental error is ±0.2% for each data point.

the filter, was set to 30 μs. This filter time is sufficiently long that rigid-phase magnetization is completely destroyed (cf. Figure 3). For the Bloch decay, a somewhat shorter pulse length of 1 μs was used, primarily to allow the use of a receiver gain setting that was also appropriate for the subsequent collection of Goldman−Shen data.

All data were recorded and stored within a single data matrix, which was then transferred to a personal computer and analyzed using the IGOR-Pro software package (Wavemetrics, Lake Oswego, OR). Steps of this analysis included sorting of free-induction decays according to mixing times, an automatic phase correction to shift spectral intensities into the real part, which were then fitted to either eq 3 (Bloch) or eq 4 (GS). The Goldman−Shen decay with the shortest mixing time (1 ms) was used as $I_{GS}(t,t_m \rightarrow 0)$. The pulse lengths and dead-time duration (5 μs) were taken into account by fitting the time-domain data using a time axis that accurately reflected the onset of data sampling after the center of the last rf pulse. Thus, relaxation during the dead time should not significantly affect the results. The use of solid echoes for data detection minimizes dead-time relaxation effects, which is more important if frequency-domain data were being analyzed. However, such sequences require longer phase cycles which can lead to prolonged measuring times for samples with sufficient signal that the number of scans are the minimum required to advance through one phase cycle. For kinetic studies, prolonged measuring times are generally undesirable.

Results and Discussion

Crystallinity. Bloch decays were measured about three times an hour for nearly 24 h while a sample of natural rubber was crystallizing at −10 °C. As described above and shown in Figure 1, these Bloch decays were immediately followed by a series of Goldman−Shen decays. A representative portion of a data set is shown in Figure 3 for the crystallization stage at 24 h. The solid lines demonstrate the quality of the fits to eq 3 (Bloch decay) or eq 4 (Goldman−Shen decays) and the validity of this approach for analyzing kinetic crystallization data. There is a slight deviation between the experimental Bloch decay and its fit, most likely related to the use of the Gaussian (eq 2) instead of the Abragam function[29] to describe the rigid component.

The fraction of rigid components ($w_{rigid} \times 100\%$), obtained by fitting the experimental Bloch decays to eq 3, is plotted as a function of crystallization time in Figure 4. The detected increase in rigid components clearly reflects the growing crystallinity. The data in Figure 4 reveal the presence of both primary and secondary crystallization events as often observed in polymers.[13] Primary crystallization occurs up to about 10 h. It can be described by the Avrami equation[33,34] with a rate constant, $k = 4.9 \times 10^{-5}$ s^{-1}, and an Avrami exponent, $\beta = 3.0$ (see dashed sigmoidal curve in Figure 4). These values compare well to those reported for crystallization of *cis*-1,4-polybutadiene at a temperature above T_g similar to that used in this study (55 K above T_g).[13] After 10 h, crystallinity continues to grow but at a much reduced rate; this region is attributed to secondary crystallization.

Note the initial rigid-component fraction in Figure 4 is not zero, but about 2.3%. The associated $T^*_{2,rigid}$ values obtained from the fits of the data from these initial stages of the crystallization are in the range 100−200 μs, which are significantly larger than the values (12−18 μs) determined for the rigid-component fraction in a well-crystallized sample. Hence, the rigid-component fraction extracted through eq 3 may not necessarily correspond to crystallites in the early stages of the crystallization. Dynamic heterogeneities, characterized by a distribution of correlation times, most certainly exist in the precrystal amorphous matrix. The more rigid components in this matrix possibly represent nascent crystal nuclei composed of locally aligned chains.[35] At later stages of the crystallization process, the rigid-component fraction determined from eq 3 largely represents polymer crystallites.

Domain Sizes. At each stage of the crystallization process, a series of Goldman−Shen decays were recorded and analyzed with eq 4 to yield the mobile-phase magnetization, $m_{mobile}(t_m)$, for different mixing times (t_m). Thus, data like those shown in Figure 5 were generated for each stage of the crystallization. The observed $m_{mobile}(t_m)$ values decreased with increasing t_m until a plateau value was reached; this plateau value of $m_{mobile}(t_m)$ is experimentally very close to the mobile-component fraction, w_{mobile}, obtained from analysis of the Bloch decay using eq 3. This is strong confirmation that virtually all crystallites are captured by the spin-diffusion process.

The average domain size was calculated from these data exactly as outlined by Mellinger et al.[32] The initial slope was extrapolated to $m_{mobile}(t_m) = 0$ to yield the intercept with the abscissa, t^*_m. These t_m* values were

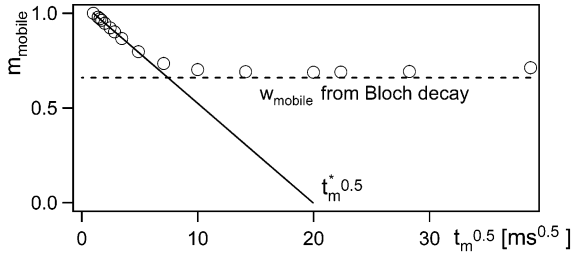

Figure 5. Mobile-phase magnetization, $m_{\text{mobile}}(t_m)$, at a given crystallization stage for natural rubber crystallizing at −10 °C. The crystallinity of the sample at the time of these particular measurements was 34%. The $m_{\text{mobile}}(t_m)$ values decrease to a plateau value, which is very close to the mobile-component fraction obtained by fitting a Bloch decay to eq 3 (w_{mobile}, shown as the horizontal dashed line). The initial slope of this plot is extrapolated to $m_{\text{mobile}}(t_m) = 0$ (shown as diagonal solid line) and the intercept with the abscissa, $(t_m^*)^{0.5}$, is used to determine the mobile-component domain size.

determined at each stage of the crystallization process and used to calculate the mobile-component domain size, d_{mobile}:[32]

$$d_{\text{mobile}} = \frac{2\epsilon}{\sqrt{\pi}}\sqrt{D_{\text{mobile}} t_m^*} \tag{5}$$

where ϵ is a constant describing the dimensionality of the diffusion process and D_{mobile} is the mobile-phase spin-diffusion coefficient. For a lamellar structure, as is likely for a polymer crystallite, $\epsilon = 1$. The spin-diffusion coefficient, D_{mobile}, was determined from the spin−spin relaxation time [obtained by approximating the $I_{GS}(t,t_m \rightarrow 0)$ decay by an exponential] using a calibration curve published by Mellinger et al.[32] Since spin diffusion occurs with significantly larger diffusion coefficients in rigid domains, the rate-determining step for equilibration of magnetization is spin diffusion through the mobile domains. Therefore, the domain sizes were estimated here using mobile-phase spin-diffusion coefficients only, while rigid-phase spin-diffusion coefficients were ignored. This assumption may lead to some inaccuracies in the absolute domain sizes. However, since D_{mobile} did not change significantly throughout the entire crystallization process, trends in domain sizes are expected to be accurate.

Spin−lattice relaxation occurs during the mixing time, but with such large time constants (T_1) that it was not necessary to correct for this effect. For example, the overall sample T_1 is 850 ms at the beginning of the crystallization process and 920 ms after 24 h. Since only $m_{\text{mobile}}(t_m)$ values for $t_m \leq 25$ ms were used to determine t_m^* (e.g., the initial slope in $m_{\text{mobile}}(t_m)$ vs $t_m^{0.5}$ plots), T_1 relaxation during this period is negligible.

Assuming identical densities for both mobile and rigid domains, the size of the detected domains, d_{mobile}, is related to the volume defined by a long period, $d = d_{\text{rigid}} + d_{\text{mobile}}$:

$$d_{\text{mobile}}^{\epsilon} = (d_{\text{mobile}} + d_{\text{rigid}})^{\epsilon} w_{\text{mobile}} \tag{6}$$

If the rigid domains are assumed to be lamellar crystals, $\epsilon = 1$ and their size (d_{rigid}) can be calculated from the mobile domain size using a simple relationship:

$$d_{\text{rigid}} = d_{\text{mobile}} \frac{w_{\text{rigid}}}{w_{\text{mobile}}} \tag{7}$$

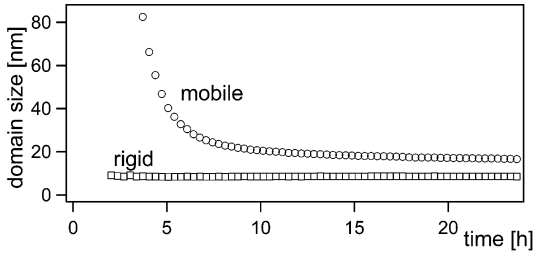

Figure 6. Sizes of mobile (○) and rigid domains (□) as a function of crystallization time for natural rubber at −10 °C. Calculated experimental error for mobile-domain data is ±0.3 nm and ±0.6 nm for rigid-domain data.

Values for $w_{\text{rigid}}/w_{\text{mobile}}$ can be directly obtained from the data shown in Figure 4. Mobile- and rigid-domain sizes were thus obtained for each stage during the crystallization and are shown in Figure 6 as a function of crystallization time.

Domain sizes were not obtained for the very early stages of the crystallization process (<2 h) because they could not be determined reliably due to the low rigid-phase content. The data of Figure 6 reveal a significant decrease for the mobile-domain size during the primary crystallization process. For 0% crystallinity the mobile-domain size is the sample size; increasing crystallinity leads to decreasing distances between the mobile amorphous domains. Interestingly, the data indicate no obvious change in the size of the rigid domains (i.e., crystallites). This can be explained by recognizing that the NMR spin-diffusion experiment only detects magnetization transport between rigid and mobile domains, not within a single domain. For a sample with increasing crystallinity (cf. Figure 4), the only explanation for a constant rigid-domain size is anisotropic growth of a three-dimensional crystal. Hence, the d_{rigid} values likely reflect the thickness of crystalline lamellae that are growing laterally (see Figure 8). Since spin-diffusion NMR does not directly detect the lateral growth of constant-thickness lamellae or spherulites, light scattering or various microscopic techniques may be used to provide complementary information. For other samples of natural rubber (stretched and cross-linked), preliminary data (not shown) reveal that d_{rigid} slightly increases during the crystallization process.

Chain Mobility and the Interphase. The above analyses have not yet made use of the $T_{2,\text{rigid}}^*$ parameter. For each stage of the crystallization process, $T_{2,\text{rigid}}^*$ values were obtained by fitting each Goldman−Shen decay to eq 4. Some representative plots of $T_{2,\text{rigid}}^*$ vs mixing time are shown in Figure 7 for five different stages of the crystallization process. These five stages are defined by their respective rigid-component fractions and are displayed as two groups. This first group represents the early stages of the crystallization process: 2.5% and 6.9% rigid domains (Figure 7A). The second group represents intermediate and late stages: 16.2, 21.2, and 32.2% rigid domains (Figure 7B). By showing $T_{2,\text{rigid}}^*$ values as functions of t_m, information on the chain mobility is provided from selective compartmentalization of the magnetization to equilibration over the entire sample. By showing $T_{2,\text{rigid}}^*$ vs t_m data for different stages of the crystallization, information on the evolving morphology can be extracted.

For the earliest stage of the crystallization ($w_{\text{rigid}} = 2.5\%$), $T_{2,\text{rigid}}^*$ decreases with increasing mixing times (● in Figure 7A) but remains significantly larger than

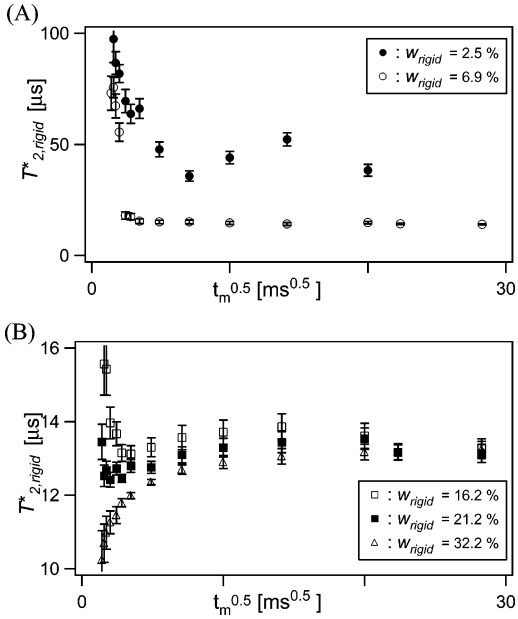

Figure 7. Chain mobility, represented by $T^*_{2,\mathrm{rigid}}$ values, vs spin-diffusion time for five different stages of the crystallization of natural rubber at −10 °C. These five stages are defined by their respective rigid-component fractions and displayed as two groups: (A) early stages of the crystallization process; (B) intermediate and late stages (the *y*-axis is scaled here to display details of $T^*_{2,\mathrm{rigid}}$ changes with spin-diffusion time).

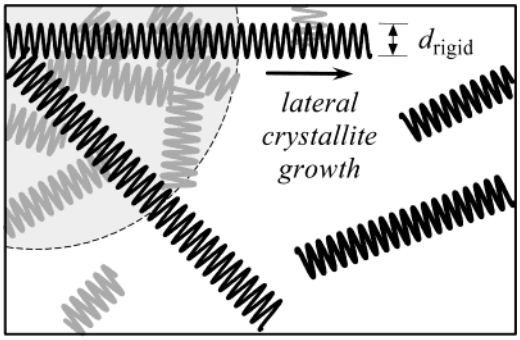

Figure 8. Schematic explanation for the increase of $T^*_{2,\mathrm{rigid}}$ with increasing t_m as observed at late stages of the crystallization, e.g., at a crystallinity of 32.2% (△ in Figure 7B). The gray area represents regions of high crystalline content and small amorphous domains in which magnetization transfer occurs on a relatively fast time scale (i.e., short t_m); since the crystals in these regions are also likely to exhibit increased perfection, they are associated with reduced values for $T^*_{2,\mathrm{rigid}}$. The white area represents regions of low crystalline content and large amorphous domains, in which magnetization transfer occurs on longer time scales (i.e., at longer t_m).

the values observed for a well-crystallized sample (10−15 μs, see Figure 7B). Hence, the selected mobile-phase magnetization diffuses into noncrystalline domains where chain rigidity increases with the distance from the selected mobile domains. These noncrystalline rigid domains may be interpreted as nascent crystal nuclei composed of locally aligned chains. At a higher rigid-component fraction (w_{rigid} = 6.9%, ○ in Figure 7A), relatively large $T^*_{2,\mathrm{rigid}}$ values are again observed for short mixing times (t_m < 4 ms). For the same short mixing times (t_m < 4 ms), the $T^*_{2,\mathrm{rigid}}$ values are smaller than those for w_{rigid} = 2.5%, signifying increased chain rigidity in the mobile domains, now interpreted as the interphase between crystallites and amorphous domains. At longer mixing times (t_m > 4 ms), the $T^*_{2,\mathrm{rigid}}$ values fall below 20 μs, which is characteristic of chains within crystalline domains. The abrupt change from $T^*_{2,\mathrm{rigid}}$ = 60 μs (interphase) to $T^*_{2,\mathrm{rigid}}$ < 20 μs (crystallite) results from using a fit function with a single relaxation constant (eq 4). If the fraction of transferred magnetization is dominated by crystalline domains, a least-squares fit will return a $T^*_{2,\mathrm{rigid}}$ value characteristic of chains within crystallites.

At intermediate and later stages of the crystallization process, all values of $T^*_{2,\mathrm{rigid}}$ are <20 μs and therefore indicative of crystalline domains (Figure 7B). Now the sample is largely composed of two phases, crystalline and amorphous. However, at a rigid-component fraction of 16.2% (□ in Figure 7B), $T^*_{2,\mathrm{rigid}}$ values initially decrease with increasing mixing time, thus indicating the presence of some interphase surrounding the crystallites in which the chains exhibit slightly higher mobility. At a rigid-component fraction of 21.2% (■ in Figure 7B), $T^*_{2,\mathrm{rigid}}$ values appear relatively uniform for different mixing times. At this and later stages of the crystallization, the interphase does not contribute significantly to the fraction of diffused magnetization. This corresponds to the closing stages of primary crystallization (see Figure 4). With the onset of secondary crystallization, $T^*_{2,\mathrm{rigid}}$ values are observed for short mixing times that are even shorter (<12 μs) than the ones associated with the major fraction of crystallites (12−14 μs) (cf. △ in Figure 7B). At these late stages of the crystallization process, some regions appear in the sample with higher crystalline density and smaller amorphous domains. The crystallites in these regions, whose lateral growth may have been arrested by impingement, nevertheless age by increasing internal perfection, a process that leads to reduced $T^*_{2,\mathrm{rigid}}$ values. Hence, selected mobile-phase magnetization diffuses more rapidly (i.e., at short mixing times) from the smaller amorphous domains into crystallites characterized by reduced $T^*_{2,\mathrm{rigid}}$ values. A schematic representation of the proposed morphology is provided in Figure 8. The NMR data reflect increasing heterogeneity in crystalline density and perfection, as expected in a sample undergoing secondary crystallization.

Conclusions

The experimental NMR approach described here provides additional insight into the nature of growing polymer crystallites as compared to previous NMR studies. In addition to overall crystallinity, the size of the growing crystallites is provided through the use of spin-diffusion experiments as a function of crystallization time. Data analysis is based on a fit function that in principle contains only two independent adjustable parameters, namely, the rigid-component fraction and chain mobility, $T^*_{2,\mathrm{rigid}}$. It can therefore be implemented easily in a fully automated fashion to yield objective results with minimal user intervention. In fact, since more than 1000 individual free-induction decays were analyzed in this study, automated batch fitting was the best approach for handling this quantity of data within a reasonable time frame. The use of eqs 3 and 4 provided the necessary robustness for these batch fits. The only potentially subjective interpretation with our approach involves the $T^*_{2,\mathrm{rigid}}$ values since a distribution of relaxation times likely exists, and only this single fit parameter is used. A $T^*_{2,\mathrm{rigid}}$ distribution could be introduced through suitable modification of eqs 3 and 4 but was

not necessary in this study to achieve high-quality fits (e.g., see Figure 3). By studying the $T^*_{2,\text{rigid}}$ values as a function of spin-diffusion time for a given stage of the crystallization, the chain mobility may be followed in the sample along the magnetization pathway from selected mobile domains to rigid domains. Such data reveal information on the evolving semicrystalline morphology as a function of crystallization time. The experimental approach poses very little demand on modern NMR hardware and may be implemented easily on low-cost benchtop NMR spectrometers.

Acknowledgment. Funding for this research was provided by the U.S.−Egypt Joint Science and Technology Board (MAN7-001-002) and the National Science Foundation (DMR-0072876). M.A.S. gratefully acknowledges financial support through the National Textile Center.

References and Notes

(1) Mark, J. E. *Polym. Eng. Sci.* **1979**, *19*, 409−413.
(2) Davis, G. T.; Eby, R. K.; Martin, G. M. *J. Appl. Phys.* **1968**, *39*, 4973−4981.
(3) Collier, J. R.; Neal, L. M. *26th Annu. Technol. Conf., Soc. Plast. Eng. Technol. Pap.* **1968**, 63−68.
(4) Vidal, A.; Haidar, B. *Elastomery* **1999**, *3*, 28−33.
(5) Peterlin, A.; Roeckl, E. *J. Appl. Phys.* **1963**, *34*, 102−106.
(6) Keller, A. *J. Polym. Sci.* **1955**, *17*, 291−308.
(7) Stein, R. S.; Cronauer, J.; Zachmann, H. G. *J. Mol. Struct.* **1996**, *383*, 19−22.
(8) Hoffmann, A.; Strobl, G. *Polymer* **2003**, *44*, 5803−5809.
(9) Cebe, P., Hsiao, B. S., Lohse, D. J., Eds.; *Scattering from Polymers: Characterization by X-rays, Neutrons, and Light*; American Chemical Society: Washington, DC, 2000; Vol. 739.
(10) Roe, R.-J. *Methods of X-Ray and Neutron Scattering in Polymer Science*; Oxford University Press: New York, 2000.
(11) Shimizu, T.; Tosaka, M.; Tsuji, M.; Kohjiya, S. *Rubber Chem. Technol.* **2000**, *73*, 926−936.
(12) Toki, S.; Sics, I.; Ran, S.; Liu, L.; Hsiao, B. S.; Murakami, S.; Senoo, K.; Kohjiya, S. *Macromolecules* **2002**, *35*, 6578−6584.
(13) Feio, G.; Cohen-Addad, J. P. *J. Polym. Sci., Part B: Polym. Phys.* **1988**, *26*, 389−412.
(14) Feio, G.; Buntinx, G.; Cohen-Addad, J. P. *J. Polym. Sci., Part B: Polym. Phys.* **1989**, *27*, 1−24.
(15) Pang, W.; Fan, C.; Zhu, Q. *Eur. Polym. J.* **2001**, *37*, 2425−2428.
(16) Kauffman, J. S.; Dybowski, C. *J. Polym. Sci., Part B: Polym. Phys.* **1989**, *27*, 2203−2209.
(17) Uehara, H.; Aoike, T.; Yamanobe, T.; Komoto, T. *Macromolecules* **2002**, *35*, 2640−2647.
(18) Brown, D. R.; Jonas, J. *J. Polym. Sci., Polym. Phys. Ed.* **1984**, *22*, 655−667.
(19) Kristiansen, P. E.; Hansen, E. W.; Pedersen, B. *Polymer* **1999**, *41*, 311−321.
(20) Kristiansen, P. E.; Hansen, E. W.; Pedersen, B. *Polymer* **2000**, *42*, 1969−1980.
(21) Hughes, C. D.; Sethi, N. K.; Baltisberger, J. H.; Grant, D. M. *Macromolecules* **1989**, *22*, 2551−2554.
(22) Ikehara, T.; Nishi, T. *Polymer* **2000**, *41*, 7855−7846.
(23) Choi, C.; Bailey, L.; Rudin, A.; Pintar, M. M. *J. Polym. Sci., Part B: Polym. Phys.* **1997**, *35*, 2551−2558.
(24) Maciel, G. E. *NATO ASI Ser., Ser. C: Math. Phys. Sci.* **1994**, *447*, 225−275.
(25) Leisen, J.; Sharaf, M. A.; Beckham, H. W. *Polym. Prepr. (Am. Chem. Soc., Div. Polym. Chem.)* **2003**, *44*, 346−347.
(26) Schmidt-Rohr, K.; Spiess, H. W. *Multidimensional Solid-State NMR and Polymers*; Academic Press: London, 1994.
(27) von Meerwall, E.; Creel, R. B.; Griffin, C. F.; DiCato, E.; Lin, F. T.; Lin, F. M. *J. Appl. Polym. Sci.* **1977**, *21*, 1489−1497.
(28) Sharma, V.; Desai, P.; Abhiraman, A. S. *J. Appl. Polym. Sci.* **1997**, *65*, 2603−2612.
(29) Abragam, A. *Principles of Nuclear Magnetism*; Clarendon: Oxford, 1961.
(30) Hansen, E. W.; Kristiansen, P. E.; Pedersen, B. *J. Phys. Chem. B* **1998**, *102*, 5444−5450.
(31) Goldman, M.; Shen, L. *Phys. Rev.* **1966**, *144*, 321−331.
(32) Mellinger, F.; Wilhelm, M.; Spiess, H. W. *Macromolecules* **1999**, *32*, 4686−4691.
(33) Avrami, M. *J. Chem. Phys.* **1939**, *7*, 1103−1112.
(34) Avrami, M. *J. Chem. Phys.* **1940**, *8*, 212−224.
(35) Ikehara, T.; Nishi, T. *Acta Polym.* **1995**, *46*, 416−419.

MA0489974